International Journal of Control, Automation and Systems 19(2) (2021) 676-686
http://dx.doi.org/10.1007/s12555-020-0138-x
ISSN:1598-6446 eISSN:2005-4092
http://www.springer.com/12555

Fractional-order Sliding Mode Constraint Control for Manipulator Systems Using Grey Wolf and Whale Optimization Algorithms

Seong-Ik Han

Abstract: This study investigates a new fractional-order nonsingular terminal sliding mode control (FTSMC) leveraging a finite-time extended state observer, a simpler prescribed control, and hybrid grey wolf optimization (GWO) combined with whale optimization algorithm (WOA) for manipulator systems. The new FTSMC system is based on an improved fractional-order terminal sliding surface. Initially, the study experimentally optimizes the dynamic parameters and gains of the controller and the observer with the help of the newly developed GWO-WOA technique. As the next step, the uncertainties including optimization error and external disturbances are estimated by the finite-time extended state observer designed using the sliding mode dynamics. Experimental results of GWO-WOA optimization and joint position tracking for a self-designed articulated manipulator prove the efficacy of the proposed control scheme.

Keywords: Experiemental grey-wolf and whale optimization, finite-time extended state observer, fractional-order nonsingular terminal sliding mode control, manipulator systems, sliding mode constraint control.

1. INTRODUCTION

The sliding mode control (SMC) approach [1] has been widely used owing to its attractive features of low sensitivity to uncertainties, fast response, and easy realization. To further improve the transient time performance and to ensure finite-time convergence, the terminal sliding mode control (TSMC) [2, 3] was developed to add a nonlinear sliding surface to the first-order sliding surface, which improve the robustness and tracking control properties. However, the singularity issue that occurs in achieving equivalent control via derivation of the terminal sliding surface limits the applicability of the TSMC approach. Thus, nonsingular terminal sliding mode controllers (NTSMCs) were designed [4, 5] to overcome the singularity issue and sustain the finite-time convergence performance.

Fractional-order TSMC (FTSMC) methods [6–12] have recently been proposed owing to their advantages of fractional-order calculus over integer-order based TSMC methods. Successful results have been obtained by applying FTSMC methods to several systems. This study proposes a new fractional-order nonsingular sliding surface that offers faster convergence compared to the previous FTSMC systems. The proposed FTSMC surface helps in avoiding the singularity issue while improving the convergence control performance, comparing to the previous methods. Additionally, the extended state observer provides feedforward compensation for modeling errors and external disturbances, by utilizing finite-time second-order sliding mode observer, thereby improving robustness to uncertainties and reducing the conservativeness of selecting switching control gains [13].

In most control systems, gains of the controller and the observer are tuned using an iterative or a trial and error method. With an increasing number of gains to be adjusted, tuning the gains becomes more time-consuming. Popular bio-inspired optimization techniques, such as particle swarm optimization (PSO) [14], ant colony optimization (ACO) [15], artificial bee colony (ABC) algorithm [16,17] have been developed to optimize unknown system parameters under minimization or maximization of the objective function. PSO is inspired by the social behavior of bird flocking. It uses a number of particles (candidate solutions) which fly around in the search space to find the best solution. ACO algorithm is inspired by the social behavior of ants in an ant colony. In fact, the social intelligence of ants in finding the closest path from the nest and a source of food is the main inspiration of this algorithm. ABC algorithm is a recently proposed optimization technique which simulates the intelligent foraging behavior of honey bees.

Manuscript received February 23, 2020; revised April 23, 2020; accepted May 20, 2020. Recommended by Associate Editor Kang-Hyun Jo under the direction of Editor-in-Chief Keum-Shik Hong. This work was supported by the National Research Foundation of Korea(NRF) grant funded by the Korea government(MSIT) (No. NRF-2018R1A2B6005128) and was supported by the Dongguk University Research Fund of 2019.

Seong-Ik Han is with the Department of Mechanical System Engineering, Dongguk University Gyeongju Campus, 123 Dongdae-ro, Gyeongju-city, Gyeongsangbuk-do, 38066, Korea (e-mail: skhan@dongguk.ac.kr).

The recently developed grey wolf optimization (GWO) technique [18–20] exhibited an improved optimization performance, in comparison with the conventional PSO and ACO techniques. However, to the best of our knowledge, control system optimization via real-time experiments has not been studied to date. Most of GWO adopted simulation optimization process. Hence, although a few applications of GWO to robotic systems have been reported [21–24], yet these optimizations have been conducted via off-line simulation. Moreover, the performance of GWO technique can enhanced though GWO showed the outperformed optimization results than other metaheuristic methods. Recently, whale optimization algorithm (WOA) [25] inspired by the bubble-net hunting strategy was studied. In [25], it was demonstrated that WOA is very competitive compared to the state-of-the-art optimization methods such as genetic algorithm (GA) [26], PSO, gravitational search algorithm (GSA) [27]. Hence, if GWO and WOA are blended such that advantages of individual methods are combined to maximize synergy effect, more enhanced method can be obtained.

Based on this motivation, in this paper, we propose a new hybrid GWO-WOA technique that offers a better optimization performance than those of both GWO and WOA techniques and we also proposed an experiment optimization learning technique. For the purposes of the study, we have executed the GWO-WOA process via real-time experiment on the manipulator system. This bio-inspired method bypasses the identification of the manipulator parameters and the time-consuming gain tuning of the controller and the observer. The experimental optimization method, which does not entirely depend on simulation optimization of conventional methods, can help in designing a faster and more effective control system for a manipulator compared to the conventional controller design systems.

Furthermore, the prescribed control method [28] was developed to constrain the tracking error in the defined boundary, guaranteeing good design performances in the control system. However, the controller structure became complicated as a result of the complex error function transformation procedures of the method. This study presents a simpler prescribed control scheme to achieve the prescribed control performance with easy realization of the controller. The control scheme simultaneously constrains both the tracking error and its rate by constraining the sliding surface, resulting in a more stable control.

The proposed control methods were applied to a self-designed articulated manipulator. The successful experimental parameter optimization procedure showed that joint position tracking worked for the proposed FTSMC surface, prescribed controller, observer, and GWO-WOA technique. The obtained results can be effectively applied to other manipulator control systems with easy realization.

2. DYNAMICS OF THE MANIPULATOR SYSTEM

2.1. Dynamics of nonlinear MIMO strict-feedback system

A nonlinear large-scale MIMO system is expressed by the following dynamic equation:

$$M(q)\ddot{q}(t)+C(q,\dot{q})\dot{q}(t)+G(q)=D(u(t))+L(t), \quad (1)$$

where q, $\dot{q}$, $\ddot{q} \in R^{n\times 1}$ denote the generalized position, velocity vector and acceleration vector, respectively; n is the degree of freedom; $M(q) \in R^{n\times n}$ is the positive definite moment of the inertia matrix; $C(q,\dot{q}) \in R^{n\times n}$ is the centripetal Coriolis matrix; $G(q) \in R^{n\times 1}$ is the gravitational vector; $L \in R^{n\times 1}$ is the 8disturbance vector including friction and external disturbance; $u \in R^{n\times 1}$ is the control input vector.

Assumption 1: There exist some finite positive constants $\rho_i > 0$, $i = M, C_j, G, L$ such that $\forall q \in R^n$, $\forall \dot{q} \in R^n$, $\|M(q)\| \le \rho_M$, $\|C(q,\dot{q})\| \le \rho_{C1} + \rho_{C2}\|\dot{q}\|$, $\|G(q)\| \le \rho_G$, and $\sup_{t\ge 0}\|L(t)\| \le \rho_L$.

Assumption 2: Two dynamic parameters of (6) can be expressed as additive perturbations $M(q) = K_M + \Delta M(q)$, $C(q) = K_C + \Delta C(q,\dot{q})$, and $G(q) = K_G\|q\| + \Delta G(q)$, where $K_M \in R^{n\times n}$, $K_C \in R^{n\times n}$, and $K_G \in R^{n\times 1}$ are constant diagonal matrices and vector, respectively.

Assumption 3: There are approximated errors δ_M and δ_G that are assumed to satisfy the following conditions:

$$\begin{cases} \|M(q)-K_M\| \le \delta_M, \\ \|C(q,\dot{q})-K_C\| \le \delta_C, \\ \|G(q)-K_G\| \le \delta_G. \end{cases} \quad (2)$$

The deadzone nonlinearity $D(u)$ is described by

$$D(u) = \begin{cases} u(t)-d_z \text{ for } u(t) \ge d_z, \\ 0 \text{ for } d_z < u(t) < d_z, \\ u(t)-d_z \text{ for } u(t) \le d_z, \end{cases} \quad (3)$$

where d_z is the width of the deadzone. Setting $u_d(t)$ as the control signal from the controller to achieve the control object for the plant without a deadzone, control signal $u(t)$ is generated in accordance with the certainty equivalence deadzone inverse [29]

$$\begin{aligned} u(t) =& D^{-1}(u_d(t)) \\ =& (u_d(t)+\hat{d}_z)p + (u_d(t)+\hat{d}_z)(1-p), \end{aligned} \quad (4)$$

where $\hat{d}_z$ is the estimate of d, $p = 1$ if $u_d(t) \ge 0$ and $p = 0$ if $u_d(t) < 0$. Because the inertia and gravity terms are more important than other dynamic terms in a manipulator system, the reduced dynamics of (1) can be expressed as

$$K_M\ddot{q}(t)+K_G = u_d(t)+N(q,t), \quad (5)$$

where $K_M \in R^{n\times n}$ and $K_G \in R^{n\times n}$ are unknown positive diagonal constant matrices and $N(q,t) \in R^{n\times 1}$ is a lumped unknown disturbance of $N(q,t) = -\Delta M(q)\ddot{q} - C(q,\dot{q})\dot{q}$. The state space representation of (1) is

$$\begin{aligned} \dot{x}_1(t) &= x_2(t), \\ \dot{x}_2(t) &= f(x(t)) + g(x(t))u_d(t) + f_d(x(t),t), \\ y(t) &= x_1(t), \end{aligned} \tag{6}$$

where $x_1(t) = q(t)$, $x_2(t) = \dot{x}_1(t)$, $f(x(t)) = -K_M^{-1}K_G$, $g(x(t)) = -K_M^{-1}$, and $f_d(x,t) = K_M^{-1}N(q,t)$ is an unknown lumped disturbance.

3. DESIGN OF CONTROLLER AND DISTURBANCE OBSERVER

3.1. Definition of sliding surface and design of controller

The PD-type ordinary function is the most popular sliding surface [1]

$$s = \dot{e} + c_0 e, \tag{7}$$

where $c_0 > 0$ is a constant diagonal matrix. To enhance the error convergence time, a terminal sliding surface function [3] was developed

$$s = \dot{e} + c_0 e + c_1 |e|^{\gamma_0} sgn(e), \tag{8}$$

where $c_1 > 0$ is a constant diagonal matrix and the terminal gain γ_0 is typically selected as $0 < \gamma_0 < 1$. c_0 and γ_0 regulate the convergence rate of the tracking error. In this case, the time derivative to obtain the equivalent control law is

$$\dot{s} = \ddot{e} + \phi_{s0}, \tag{9}$$

where $\phi_{s0} = c_0 + c_1\gamma_0 dia(|e_i|^{\gamma_0-1})\dot{e}$. However, ϕ_{s0}can be singular if $\dot{e} \neq 0$ and $e = 0$ because $0 < \gamma_0 < 1$ in (9), and $diag(|e_i|^{\gamma_0-1})\dot{e}$ becomes $\dot{e}/diag(|e_i|^{1-\gamma_0})$. Thus, to prevent the singularity of the terminal sliding surface, it was changed to nonsingular type

$$s = \dot{e} + c_0 e + c_1 |e|^{\gamma_1} sign(e), \tag{10}$$

where $\gamma_1 > 2$. However, in this case, degradation of convergence performance is inevitable when $\gamma_1 > 2$. Therefore, to make the system achieve faster convergence and reach the equilibrium point in finite time without singularity, nonsingular fractional-order terminal sliding mode surfaces were developed [7, 8, 11]

$$\sigma = s + c_2 s^{\gamma_2} + c_3 \dot{s}^{\gamma_3}, \tag{11}$$

$$\sigma = \dot{s} + c_3 D^{\alpha_3 - 1}[|s|^{\gamma_3} sign(s)], \tag{12}$$

$$\sigma = \dot{s} + c_2 D^{\alpha_2}[|s|^{\gamma_2} sign(s)] + c_3 D^{\alpha_3 - 1}[|s|^{\gamma_3} sign(s)], \tag{13}$$

where the Riemann-Liouville definition of fractional derivative is given as follows [30]:

$${}_0D_t^{\alpha} f(t) = \frac{1}{\Gamma(n-\alpha)} \frac{d^n}{dt^n} \int_0^t \frac{f(\tau)}{(t-\tau)^{\alpha-n+1}} d\tau, \tag{14}$$

where n is the first integer larger than α, i.e., $n-1 \leq \alpha < n$ and Γ is the Gamma function. This study proposes a new sliding surface

$$\sigma = D^{\alpha_1} s + D^{\alpha_2 - 1}[c_2 s + c_3 |s|^{\gamma_3} sign(s)], \tag{15}$$

where c_2 and c_3 are positive constant diagonal matrices, and $0 < \alpha_i \leq 1, 1 < \gamma_2 < 2$, and $\gamma_3 > 1$ are constants. For mathematical comparison of the nonsingular sliding surface only between (13) and (14), when $\sigma = 0$ with the case of $s > 0$, (13) and (15) can be written as

$$s = -c_2 D^{\alpha_2 - 1} s^{\gamma_2} - c_3 D^{\alpha_3 - 2} s^{\gamma_3}, \tag{16}$$

$$s = -c_2 D^{\alpha_2 - \alpha_1 - 1} s - c_3 D^{\alpha_2 - \alpha_1 - 1} s^{\gamma_3}. \tag{17}$$

Since $\gamma_i > 1$, (17) has more flexibility to select the tuning gain than (16) to make the surface to be zero and can be converged to zero more rapidly than (16). To be shown in graphical behavior, for $\sigma(t) = 0$, the selected parameters were $\alpha_1 = 0.2$, $\alpha_2 = 0.2$, $\alpha_3 = 0.2$, $c_2 = 5$, $c_3 = 2$, $\gamma_1 = 1.5$, $\gamma_2 = 1.5$, and $\gamma_3 = 1.5$ under the initial condition $s(0) = 1$.

Fig. 1 shows that the proposed sliding surface offers the fastest convergence compared with other surfaces. Taking the time derivative of (15) and applying $D^{-\alpha_1}$ to both sides of (15), we obtain

$$\begin{aligned} D^{\bar{\alpha}_1}\sigma =& \dot{s} + D^{\bar{\alpha}_2}[c_2 s + c_3 |s|^{\gamma_3} sign(s)] \\ =& f(x,t) + g(x)u_d(t) - \ddot{y}_d(t) + d(x,t) + \phi_{s2}, \end{aligned} \tag{18}$$

where $D^{\bar{\alpha}_1}$ and $D^{\bar{\alpha}_2}$ are represented by $D^{1-\alpha_1}$ and $D^{\alpha_2-\alpha_1}$, respectively, and $\phi_{s2} = \phi_{s1} + D^{\bar{\alpha}_2}[c_2 s + c_3(|s|^{\gamma_3} \cdot sign(s)]$.

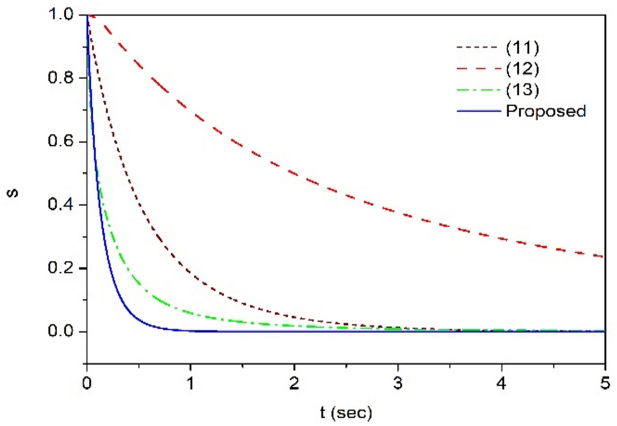

Fig. 1. Convegence of $s(t)$.

To design a controller, the following is defined:

$$D^{\bar{\alpha}_1}\sigma = -k_1\sigma - k_2|\sigma|^{1/2}sign(\sigma) - k_3\sigma(|\sigma|+\varsigma)^{-1}, \tag{19}$$

where $k_1\sigma$ corresponds to the control to attract the states to the sliding surface, $k_3\sigma(|\sigma|+\varsigma)^{-1}$ acts the states to remain within the sliding surface, and $k_2|\sigma|^{1/2}sign(\sigma)$ is the finite-time control term. Considering (18) and (19), a fractional-order nonsingular sliding mode control law is designed as

$$\begin{aligned} u_d(t) =& g^{-1}(x)[-f(x,t)+\ddot{y}_d(t)-d(x,t)-\phi_{s2}] \\ & -k_1\sigma - k_2|\sigma|^{1/2}sign(\sigma) - k_3\sigma(|\sigma|+\varsigma)^{-1}, \end{aligned} \tag{20}$$

where k_i, $i = 1, 2, 3$, are positive constant diagonal matrices and $\varsigma > 0$ is a constant. However, the disturbance $d(x,t)$is not known a priori, so a disturbance observer to estimate $d(x,t)$ is considered.

3.2. Design of an extended state observer

The disturbance for the augmented state $d(x,t) = f_d(t)$ in (6) is estimated by using the fractional extended state observer From (10), the following dynamics can be considered

$$\dot{s} = f(x,t) + g(x)u_d(t) - \ddot{y}_d(t) + d(x,t) + \phi_{s1}. \tag{21}$$

A fractional-order extended state observer can be considered as

$$\begin{aligned} \dot{\hat{s}}(t) =& f(x,t) + g(x)u_d(t) - \ddot{y}_d(t) + \phi_{s1} + \hat{d}(x,t) \\ & + \kappa_1|\chi|^{\gamma_\chi}sign(\chi) + \kappa_2\chi, \end{aligned} \tag{22}$$

$$\dot{\hat{d}}(x,t) = \kappa_3 sign(\chi) + \kappa_4\chi, \tag{23}$$

where $\chi = s - \hat{s}$ is the auxiliary error variable vector, $\gamma_\chi > 1$ is a constant, κ_i are positive constant matrices, and $\hat{s}(t)$ and $\hat{d}(x,t)$ are estimates of $s(t)$ and $d(x,t)$, respectively. An error dynamics is considered for χ by defining the system's input $\tilde{d}(x,t)$ such that the system converges to the origin of the phase plane of $\chi - \dot{\chi}$ in finite-time with a twisting motion

$$\dot{\chi}(t) = -\kappa_1|\chi(t)|^{\gamma_\chi}sign(\chi(t)) - \kappa_2\chi(t) + \tilde{d}(x,t), \tag{24}$$

$$\dot{\tilde{d}}(x,t) = -\kappa_3 sign(\chi(t)) - \kappa_4\chi(t) + \dot{f}_d(x,t), \tag{25}$$

where $\tilde{d}(x,t) = d(x,t) - \hat{d}(x,t)$ is the estimation error. Thus, in finite time, $\tilde{d}(x,t) \to 0$ if $\chi(t) \to 0$. In (25), $\dot{f}_d(x,t)$ is the uncertain term that satisfies the condition, $|\dot{f}_d(x,t)| \le \delta_{d1} + \delta_{d2}|\chi|$ for positive constants δ_{d1} and δ_{d2}.

3.3. Design of prescribed sliding surface control

Considering the smooth decreasing positive performance functions $p_c(t)$

$$p_c(t) = (p_{c0} - p_{cs})e^{-at} + p_{cs}, \tag{26}$$

where $p_{c0} > 0$, $p_{cs} > 0$, $a > 0$, and $\lim_{t\to\infty} p_c(t) = p_{cs}$ are constant for a predefined tracking performance, transient performance is guaranteed by the prescribed constraint conditions of

$$-p_c(t) < \sigma(t) < p_c(t). \tag{27}$$

Constraint function for the sliding surface is expressed as

$$\Phi_c = \tan\left(\frac{\sigma(t)}{p_c(t)}\right), \tag{28}$$

where Φ_c is a smooth function that satisfies the following condition:

$$0 \le \Phi_c < \kappa_c\tan(1), \tag{29}$$

where $\lim_{\sigma>0\to p_c}\Phi_c = \tan(1)$ and $\lim_{\sigma<0\to -p_c}\Phi_c = \tan(1)$. Using (29), the constraining controller can be constructed as follows:

$$u_c = -k_4\Theta_c\sigma, \tag{30}$$

where $\Theta_c = \Phi_c sign(\sigma)$ and $k_4 > 0$ is a constant. As the next step, a fractional-order finite-time sliding mode controller, with an error surface constraint, is designed

$$\begin{aligned} u_d(t) =& g(x)^{-1}[-f(x,t)+\ddot{y}_d(t)-\hat{d}(x,t)-\phi_{s1}] - k_1\sigma \\ & - k_2|\sigma|^{1/2}sign(\sigma) - k_3\sigma(|\sigma|+\varsigma)^{-1} \\ & + g(x)^{-1}u_c. \end{aligned} \tag{31}$$

4. STABILITY ANALYSIS

Theorem 1: Consider the perturbed dynamics in (21), (22), and (6), with the controller expressed in (31). The errors $\chi(t)$ and $\tilde{d}(x,t)$ in (24) and (25) converge to zero in finite time if the gains κ_i satisfy the following conditions:

$$\begin{aligned} & \kappa_1 > 0, \quad \kappa_2 > \frac{1}{2}\sqrt{2\delta_{d2}}, \quad \kappa_3 > \delta_{d1}, \\ & \kappa_4 > \left[\frac{\left(\frac{1}{2}\kappa_1^3(2\kappa_2^2 - \delta_{d2}) + (\frac{5}{2}\kappa_2^2 + \delta_{d2})\right)p_1}{\left(p_1 - \frac{1}{2}\kappa_1^3\right)} - \frac{1}{2}\kappa_2\right], \\ & p_1 = \kappa_1\left(\frac{1}{4}\kappa_1^2 - \delta_{d1}\right) + \frac{1}{2}\kappa_1\left(2\kappa_3 + \frac{1}{2}\kappa_1^2\right). \end{aligned} \tag{32}$$

Proof: This proof is similar to that in [13] and then is proved as follows: The Lyapunov function is defined as $V_\xi = \xi^T\Theta\xi$, where

$$\xi = \begin{bmatrix} |\chi|^{1/2}sign(\chi) & \chi & \tilde{d} \end{bmatrix}^T,$$

$$\Theta = \frac{1}{2}\begin{bmatrix} (4\kappa_3 + \kappa_1^2) & \kappa_1\kappa_2 & -\kappa_1 \\ \kappa_1\kappa_2 & (2\kappa_4 + \kappa_2^2) & -\kappa_2 \\ -\kappa_1 & -\kappa_2 & 2 \end{bmatrix}.$$

The time derivative along the trajectories of the system with (24) and (25) is given by

$$\dot{V}_\xi = -\frac{1}{|\chi|^{1/2}}\xi^T\Psi_1\xi - \xi^T\Psi_2 + \psi_1^T\xi, \tag{33}$$

where $\psi_1 = [-\delta_{d1}\kappa_1 \;\; -\delta_{d1}\kappa_2 \;\; 0]^T$. By using the bounds of $\dot{f}_d(x,t)$, it follows that

$$\psi_1^T\xi \le \frac{1}{|\chi|^{1/2}}\xi^T\Delta_1\xi + \xi^T\Delta_2\xi, \tag{34}$$

where

$$\Delta_1 = \begin{bmatrix} \delta_{d1}\kappa_1 & 0 & 0 \\ 0 & \delta_{d2}\kappa_1 & 0 \\ 0 & 0 & 0 \end{bmatrix}, \;\; \Delta_2 = \begin{bmatrix} \delta_{d1}\kappa_2 & 0 & 0 \\ 0 & \delta_{d2}\kappa_2 & 0 \\ 0 & 0 & 0 \end{bmatrix}.$$

Equation (31) can then be rewritten as

$$\dot{V}_\xi = -\frac{1}{|\chi|^{1/2}}\xi^T(\Psi_1 - \Delta_1)\xi - \xi^T(\Psi_2 - \Delta_2)\xi. \tag{35}$$

$\Psi_1 > \Delta_1$ if $\kappa_1 > 0$, $\kappa_2 > \frac{1}{2}\sqrt{2\delta_{d2}}$, $\kappa_3 > \delta_{d1}$, and $\kappa_4 > \left[\frac{\left(\frac{1}{2}\kappa_1^3(2\kappa_2^2-\delta_{d2})+(\frac{5}{2}\kappa_2^2+\delta_{d2})\right)p_1}{\left(p_1-\frac{1}{2}\kappa_1^3\right)} - \frac{1}{2}\kappa_2\right]$. Next, $\Psi_2 > \Delta_2$ if $\kappa_2 > 0$, $\kappa_3 > \delta_{d1} - 2\kappa_1^2$, and $\kappa_4 > \kappa_2^2 + \delta_{d2}$. Considering the upper bounds for $\Psi_1 > \Delta_1$ and $\Psi_2 > \Delta_2$, the parameter conditions in (32) guarantee the conditions of both $\Psi_1 > \Delta_1$ and $\Psi_2 > \Delta_2$. Thus, the global asymptotic stability and the finite-time convergence are guaranteed and therefore, $\chi(t)$ and $\tilde{d}(t)$ converge to zero in finite-time. □

Assumption 4 [6]**:** The following condition is satisfied:

$$\left|\sum_{j=1}^{\infty}\frac{\Gamma(1+\bar{\alpha}_2)}{\Gamma(1-j+\bar{\alpha}_2)\Gamma(1+j)}D^j\sigma D^{\bar{\alpha}_2-j}\sigma\right| \le \eta|\sigma|, \tag{36}$$

where η is a positive constant.

Lemma 1: Based on the Assumption 4, the following condition is satisfied:

$$\left|\sum_{j=1}^{\infty}\frac{\Gamma(1+\bar{\alpha}_2)}{\Gamma(1-j+\bar{\alpha}_2)\Gamma(1+j)}D^j\sigma D^{\bar{\alpha}_2-j}\sigma\right| \le \eta|\sigma|^\zeta, \tag{37}$$

where ζ is a positive constant.

Proof: The following condition is obtained due to $\zeta > 1$: If $|\sigma| < 1$, it follows that

$$\left|\sum_{j=1}^{\infty}\frac{\Gamma(1+\bar{\alpha}_2)}{\Gamma(1-j+\bar{\alpha}_2)\Gamma(1+j)}D^j\sigma D^{\bar{\alpha}_2-j}\sigma\right| \le \eta|\sigma|^\zeta < \eta|\sigma|. \tag{38}$$

If $|\sigma| \ge 1$, it follows that

$$\left|\sum_{j=1}^{\infty}\frac{\Gamma(1+\bar{\alpha}_2)}{\Gamma(1-j+\bar{\alpha}_2)\Gamma(1+j)}D^j\sigma D^{\bar{\alpha}_2-j}\sigma\right| \le \eta|\sigma| \le \eta|\sigma|^\zeta. \tag{39}$$

Therefore, regardless of the$|\sigma|$, (37) is obtained if the Assumption 4 is satisfied. □

Theorem 2: Consider the dynamic system given in (6), the sliding mode surfaces in (15), and control input in (31). The second sliding mode surface converges to the origin $\sigma = 0$ in finite-time $t_{\sigma_f} \le [V_\sigma^{\bar{\alpha}_1-2}(t_{\sigma_r})/((k_2-\eta)\Lambda)]^{1/(1-\bar{\alpha}_1)}$, where t_{σ_r} is the time to reach from $\sigma \neq 0$ to $\sigma = 0$, and k_2, η, and Λ are positive constants.

Proof: By using Lemma 1 and defining the Lyapunov function as $V_\sigma = \frac{1}{2}\sigma^T\sigma$, applying the fractional operator $D^{\bar{\alpha}_1}$ to the function with (16), and setting $\zeta = \frac{3}{2}$, one obtains

$$\begin{aligned} D^{\bar{\alpha}_1}V_\sigma =& \sigma D^{\bar{\alpha}_1}\sigma \\ &+ \left|\sum_{j=1}^{\infty}\frac{\Gamma(1+\bar{\alpha}_1)}{\Gamma(1-j+\bar{\alpha}_1)\Gamma(1+j)}D^j\sigma D^{\bar{\alpha}_1-j}\sigma\right| \\ \le& \sigma[f(x,t) + g(x)u_d(t) - \ddot{y}_d(t) + d(x,t) \\ &+ \phi_{s2}] + \eta|\sigma|^{3/2}. \end{aligned} \tag{40}$$

Substituting (31) into (40), one obtains

$$\begin{aligned} D^{\bar{\alpha}_1}\dot{V}_\sigma \le& \sigma^T[\tilde{d}(x,t) - k_2|\sigma|^{1/2}sign(\sigma) \\ &- k_3\sigma(|\sigma|+\varsigma)^{-1} - k_4\Theta_c\sigma] + \eta|\sigma|^{3/2} \\ \le& \sigma^T[-k_1\sigma - k_2|\sigma|^{1/2}sign(\sigma)] - \Theta_c|\sigma|^2 \\ &+ \eta|\sigma|^{3/2} + |\sigma|\left|\tilde{d}(x,t)\right| - k_3\sigma^T\sigma(|\sigma|+\varsigma)^{-1} \\ \le& -k_1\sigma^T\sigma - k_2|\sigma|^{3/2} + \eta|\sigma|^{3/2} \\ &- |\sigma|\left(k_3|\sigma|(|\sigma|+\varsigma)^{-1} - \delta_{dm}\right). \end{aligned} \tag{41}$$

In (41), if k_3 is selected such that $k_3|\sigma|(|\sigma|+\varsigma)^{-1} \ge \delta_{dm}$ is satisfied with$\left|\tilde{d}'(x,t)\right| \le \delta_{dm}$, the condition

$$D^{\bar{\alpha}_1}V_\sigma \le -(k_2-\eta)|\sigma|^{3/2}, \tag{42}$$

where k_2 is selected appropriately such that $k_2 > \eta$ is satisfied. Taking fractional-order integral of (42) from reaching time t_{σ_r} to settling time t_{σ_f}, one obtains

$$V_\sigma(t_{\sigma_f}) - V_\sigma(t_{\sigma_r})\frac{t_{\sigma_f}^{\bar{\alpha}_1-2}}{\Gamma(\bar{\alpha}_1-1)} \le -(k_2-\eta)D^{1-\bar{\alpha}_1}|\sigma|^{3/2}. \tag{43}$$

Based on [6], there is a positive constant Λ such that $D^{1-\bar{\alpha}_1}|\sigma|^{3/2} \ge \Lambda$. (43) can be expressed as

$$-V_\sigma(t_{\sigma_r})\frac{t_{\sigma_f}^{\bar{\alpha}_1-2}}{\Gamma(\bar{\alpha}_1-1)} \le -(k_2-\eta)\Lambda, \tag{44}$$

because $V_\sigma(t_{\sigma_f}) = 0$ due to $\sigma = 0$ at t_{σ_f} in (41). Thus, one obtains

$$t_{\sigma_f} \le \left(\frac{V_\sigma^{\bar{\alpha}_1-2}(t_{\sigma_r})}{\Gamma(\bar{\alpha}_1-1)(k_2-\eta)\Lambda}\right)^{1/(2-\bar{\alpha}_1)}. \tag{45}$$

Therefore, based on the Theorem 1, the tracking error $e(t)$ and sliding surface $s(t)$ also converge to zero in finite-time as does the sliding surface $\sigma(t)$. □

5. EXPERIMENTAL PARAMETER OPTIMIZATIOIN USING HYBRID GREY WOLF AND WHALE ALGORITHM

5.1. Hybrid grey-wolf and whale optimization algorithm

The GWO technique [18–24] is inspired by nature and follows the leadership and hunting mechanism of the grey wolf in its environment. Four types of grey wolves are engaged to optimize unknown parameters: alpha (α_w), beta (β_w), omega (ω_w), and delta (δ_w). In the entire search space, the three best located alpha, beta, and delta grey wolves help in directing the remaining omega wolves toward the best location. The following equations are considered to mathematically model the encircling behavior:

$$\vec{D}_g = \left|\vec{C}_g\vec{X}_p(t) - \vec{X}_g(t)\right|, \tag{46}$$

$$\vec{X}_g(t+1) = \vec{X}_p(t) - \vec{A}_g\vec{D}_g, \tag{47}$$

where t indicates the current iteration, $\vec{A}_g$ and $\vec{C}_g$ are coefficient vectors, $\vec{X}_p$ is the position vector of the prey, and $\vec{X}_g$ indicates the position vector of the grey wolf. The vectors $\vec{A}_g$ and $\vec{C}_g$ are calculated as follows:

$$\vec{A}_g = 2\vec{a}\vec{r}_1 - \vec{a}, \vec{C}_g = 2\vec{r}_2, \tag{48}$$

where $\vec{a}$ are linearly reduced from 2 to 0 over the course of iteration, r_1 and r_2 are random vectors in [0, 1]. The following different mathematical equations are utilized to evaluate the hunting action of the prey:

$$\vec{D}_i = \left|\vec{C}_{gj}\vec{X}_i - \vec{X}_g\right|, i = \alpha_w, \beta_w, \delta_w, \quad j = 1,2,3, \tag{49}$$

$$\vec{X}_{gi} = \vec{X}_i - \vec{A}_{gj}(\vec{D}_i), i = \alpha_w, \beta_w, \delta_w, \quad j = 1,2,3, \tag{50}$$

$$\vec{X}_g(t+1) = \frac{\vec{X}_{g\alpha_w} + \vec{X}_{g\beta_w} + \vec{X}_{g\delta_w}}{3}. \tag{51}$$

Humpback whales use a unique hunting method called the bubble-net feeding method [25]. Humpback whales prefer to hunt school of krill or small fish close to the surface. The updating behavior of humpback whales when encircling their prey is represented by the following equations:

$$\vec{D} = \left|\vec{C}\vec{X}_w^*(t) - \vec{X}_w(t)\right|, \tag{52}$$

$$\vec{X}_w(t+1) = \vec{X}_w^* - \vec{A}_w \cdot \vec{D}_w, \tag{53}$$

where t indicates the current iteration, $\vec{A}_w$ and $\vec{C}_w$ are coefficient vectors, $\vec{X}_w^*$ is the position vector of the best solution, $\vec{X}_w$ is the position vector of the humpback whale, and $\cdot$ represents an element-by-element multiplication. X_w^* is updated in each iteration if there is a better solution. Vectors $\vec{A}_w$ and $\vec{C}_w$ are similarly calculated by (48). The humpback whales swim around the prey within a shrinking circle and along a spiral path simultaneously. Including this behavior and assuming a probability of 50% to choose either the shrinking encircling mechanism or the spiral model to update the position of whales during optimization leads to the following mathematical model:

$$\vec{X}_w(t+1) = \begin{cases} \vec{X}_w^*(t) - \vec{A}_w \cdot \vec{D}_w \text{ if } p < 0.5, \\ \vec{D'}_w \cdot e^{bl} \cdot \cos(2\pi t) + \vec{X}_w^*(t) \text{ if } p \geq 0.5, \end{cases} \tag{54}$$

where $\vec{D}'_w = \left|\vec{X}_w^*(t) - \vec{X}_w(t)\right|$ indicates the distance of the ith whale to the prey, b is a constant for defining the shape of the logarithmic spiral,l is a random number in $[-1, 1]$, and p is a random number in $[0, 1]$. In this study, we combine the GWO and WOA optimization techniques such that

$$\vec{X}_g(t+1) = \frac{\vec{X}_w + \vec{X}_{g\beta_w} + \vec{X}_{g\delta_w}}{3} \tag{55}$$

by introducing (55) into (51) instead of$\vec{X}_{g\alpha_w}$. This hybrid technique improves the optimization performance over the performance of the GWO and WOA techniques individually.

5.2. Experimental optimization strategy of the manipulator parameters and the proposed controller and observer

The unknown parameters of the manipulator and tuning gains of the controller and observer were experimentally optimized by the proposed GWO-WOA technique. We designed the articulated manipulator with dynamixel servo motors. Fig. 2 shows the 3D CAD drawing and photograph of the manipulator.

In this study, only three links among them were selected to apply the control system excluding the wrist axis. The specifications of the manipulator dynamics with the dynamixel servo motors (XM540-W270-R) assembled in each joint are given as, $m_1 = 1.2$ kg, $m_2 = 0.6$ kg, $m_3 = 0.7$ kg, $l_1 = 0.1$ m, and $l_2 = l_3 = 0.2$ m. To control the dynamixel servo motor equipped in each joint of the manipulator, the R+ manager was installed. The torque mode

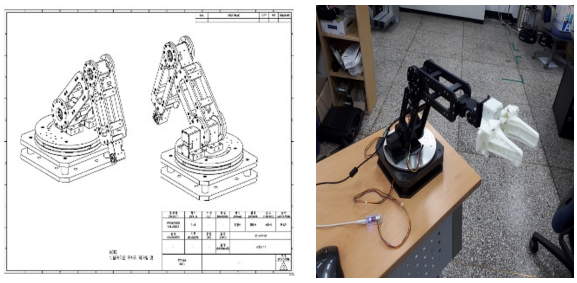

(a) (b)

Fig. 2. Self-designed articulated manipulator system. (a) 3D drawing. (b) Photograph.

of the dynamixel motor was set and the data communication line via the USB serial port connected to each joint motor was checked. Next, the path in the Matlab package was added and support packages such as DynamixelSDK-master and the MinGW-w64 C/C++ compiler were installed. After setting the torque mode, we executed the following Matlab code to create the object of the *slDxl* class:

myDxl = slDxl('COMi', 57600);
myDxl.doEnableTorque(i); i =1,2,3

To release the torque mode, we executed the following command:

myDxl.doDisableTorque(i), i = 1,2,3.

These torque control commands were used in the process of the experimental GWO-WOA optimization and end-effector tracking experiment. The GWO-WOA pseudo code with the experimental optimization is given as follows:

Initialize the grey wolf and whale population $X_{g\beta_{wi}}$, $X_{g\delta_{wi}}$, and X_{wi}*(i=1,2,3) % i is a link number*
Initialize a, A, C, l , and p
Calculate the fitness of each search agent
X_{wi}*= the best search agent of whale*
$X_{g\beta_{wi}}$*= the second best search agent of grey wolf*
$X_{g\delta_{wi}}$*= the third best search agent of grey wolf*
while ($t <$ *Max number of epoch*)
myDxl.doEnableTorque(*i*)
for each search agent
Update a, A, C, l, and p
Update the position of the current search agent by the above equations
Calculate the fitness of all search agents using real-time
Matlab simulink
fitness = simulink-script- file(X_{gi4})
UpdateX_{wi},$X_{g\beta wi}$, *and*$X_{g\delta_{wi}}$
myDxl.doDisableTorque(*i*) $t = t+1$ *end while*
myDxl.doEnsableTorque(*i*)
return$X_{gi} = (X_{wi} + X_{g\beta_{wi}} + X_{g\delta_{wi}})/3.$

The controller used in the GWO-WOA was implemented by the Matlab real-time simulink model.

5.3. Results of experimental GWO-WOA optimization

The performance criteria used to define the objective function were selected as the minimization of the integral time absolute error (ITAE). Some important features of ITAE are that (a) the absolute error minimizes the percentage of overshoot, and (b) the time multiplication term minimizes the oscillations in the further response and effectively reduces settling time. The ITAE-based objective function is expressed as

Table 1. Final ITAE value of the WOA, GWO, GWO-WOA technique.

Technique	Link 1	Link 2	Link 3
WOA	0.032 (100%)	0.39 (100%)	0.023 (100%)
GWO	0.027 (84%)	0.029 (74%)	0.019 (83%)
GWO-WOA	0.024(75%)	0.022(56%)	0.018 (78%)

$$Objective\_function = ITAE = \int t\,|e(t)|\,dt. \qquad (56)$$

The objective function was minimized such that $18 \times no.\,of\,link = 36$ constraint conditions with the upper and lower bounds for the unknown manipulator dynamics and tuning gains of controller and observer: K_{Mi}, K_{Gi}, $\hat{d}_{zi}$, c_{ji}, $j = 0, 1, 2, 3$, $i = 1, 2, 3$, α_{ji}, $j = 1, 2$, $i = 1, 2, 3$, γ_{ji}, $j = 1, 3$, $i = 1, 2, 3$, k_{ji}, $j = 1, 2, 3$, $i = 1, 2, 3$, κ_{ji}, $j = 1, 2, 3, 4$, $i = 1, 2, 3$. The prescribed control tuning gain k_{4i} was not optimized because the special condition must be considered in this control case. The test position command inputs for optimization were selected as $q_{d1} = 0.125\sin(1.26t) + 1.84$ rad, $q_{d2} = 0.125\sin(1.26t) + 2.76$ rad, and $q_{d2} = 0.125\sin(1.26t) + 3.07$ rad. The number of agent in each link was set as 5 and maximum epoch was 30.

Fig. 3(a) shows the tracking outputs in each link until 5 epochs optimized by the GWO-WOA technique. It can be shown that the tracking performances increasingly improved according to increase in epoch number in all links. In the final epoch, more, all parameters are converged to the optimized values. Fig. 3(b) shows the fitness value of the GWO, WOA, and GWO-WOA techniques in each link. First of all, the convergence speed is very important performance in the optimization technique. As seen Figs. 3(d), (e), and (f), the GWO-WOA reaches the minimum ITAE values most rapidly within about 10 epochs than the other techniques. Next, it is seen that the size of ITAE maintains until the end of epoch. Table 1 presents the obtained ITAE fitness values of three techniques. In Table 1, the ITAE size of the proposed method deceases until maximum 56% of that of WOA.

Since these metaheuristic methods use the random values in initial steps, the final estimation results may vary a little in each estimation experiment. Therefore, several iterational optimization experiments were reprated and the average values are summarized in Table 1. From these results, it can be shown that the proposed GWO-WOA technique outperforms compared with other two techniques.

However, the main difficulty of the proposed GWO-WOA including GWO technique is the setting of the optimization boundaries of each parameter. Now, the boundary setting can't help depending on the individual experience and engineering sensitivity. Further setting method for the boundary setting of the parameters is necessary in next time.

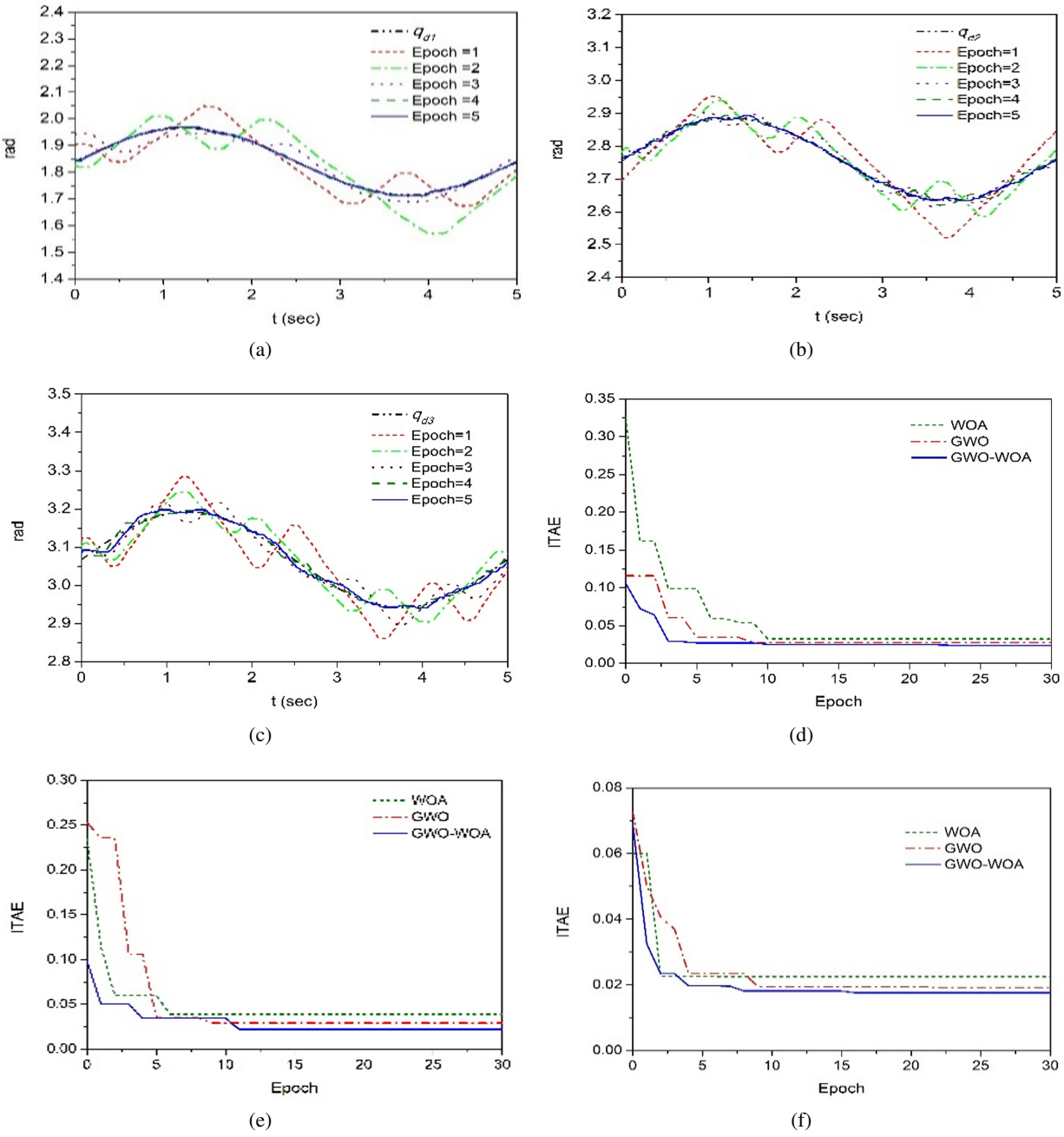

Fig. 3. Experimental optimization results in each link. Tracking output for the testing command inputs according to optimizing epochs of the GWO-WOA: (a) link 1, (b) link2, and (c) link 3. Fitness values of the GWO, WOA, and GWO-WOA techniques: (d) link 1, (e) link 2, and (f) link 3.

6. EXPERIMENTAL RESULT FOR THE END-EFFECTOR POSITIONING OF THE MANIPULATOR

Based on the optimized control gains, the end-effector tracking experiment for the manipulator was executed. For comparison of the control performance, three controllers were designed: the terminal nonsingular sliding mode controller (TSMC) based on (10), which was designed as

$$u_d(t) = g^{-1}(x)[-f(x,t) + \ddot{y}_d(t) - \hat{d}(x,t) - \phi_{s1}] - k_1 s - k_2 |s|^{1/2} sign(s) - k_3 s(|s| + \varsigma)^{-1}, \quad (57)$$

the fractional order terminal nonsingular sliding mode controller (FTSMC) without prescribed control and the fractional order terminal nonsingular sliding mode con-

Table 2. Optimized controller parameters.

Joint	Optimized values of each parameter
Joint1	$K_{M1}=0.045$, $K_{C1}=0$, $K_{G1}=0$, $D_{z1}=0.11$, $c_{21}=5.3$, $c_{31}=6.5$, $k_{11}=0.13$, $k_{21}=14.7$, $k_{31}=1.64$, $\alpha_{11}=0.31$, $\alpha_{21}=0.29$, $\gamma_{31}=1.03$
Joint2	$K_{M2}=0.001$, $K_{C2}=0.005$, $K_{G2}=0.1$, $c_{22}=1.3$, $c_{32}=1$, $k_{12}=5$, $k_{22}=10$, $k_{32}=19$,]-0.2pc] $\alpha_{12}=0.23$, $\alpha_{22}=0.4$, $\gamma_{32}=1.1$
Joint3	$K_{M3}=0.006$, $K_{C3}=0.0014$, $K_{G3}=0.14$, $c_{32}=1.66$, $c_{32}=10$, $k_{13}=9$, $k_{23}=1.7$, $k_{33}=1$, $\alpha_{13}=0.29$, $\alpha_{23}=0.15$, $\gamma_{33}=1.05$

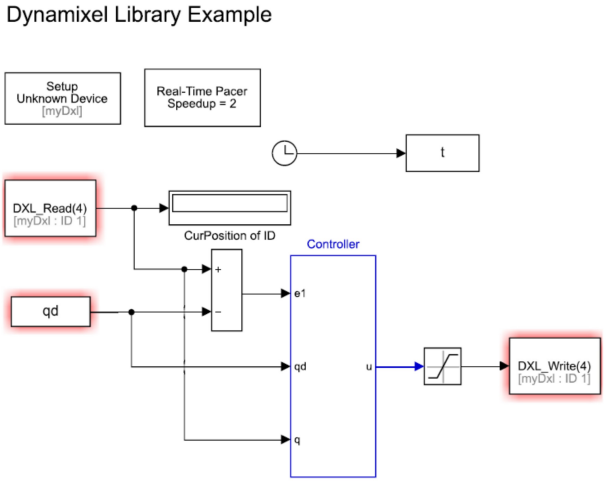

Fig. 4. Block diagram of the implemented controller.

troller with prescribed control (PFTSMC). The parameters and gains for the prescribed control were selected as $p_{c0i}=3.834$, $p_{s1}=1.227$, $p_{s2}=p_{s2}=0.614$, $a_1=2$, $a_2=a_3=1$, and $k_{41}=12$, $k_{42}=20$, $k_{43}=5$. The optimized controller parameters are presented in Table 2.

Remark 1: The fractional-order parameters in Table 2 are much sensitive to the control performance than others because these determine the property of the sliding surfaces.

Fig. 4 shows the block diagram constructed by the Matlab simulink realtime package combined with the dynamixel motor library.

The desired position of the end-effector in Cartesian coordinate was selected as follows:

$$x_r(t)=400\text{ mm},\ \ y_r(t)=-195+19.5t\text{ mm},$$
$$z_r(t)=-120\sin(0.016(y(t)+195))+330\text{ mm}. \tag{58}$$

The sampling frequency was 100Hz. The experimental results of the articulated manipulator system are presented in Fig. 6 for the tracking command trajectory given in (58) and Fig. 5. Fig. 5(b) represents the inverse position of each joint for the rectangular position of the end-effector given

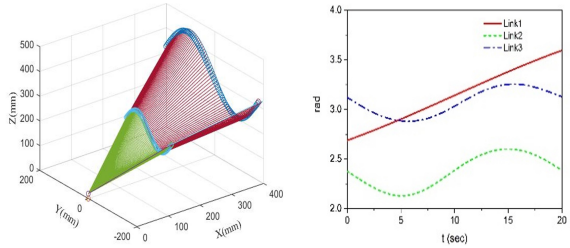

(a) (b)

Fig. 5. Cartesian position of the end-effector and inverse joint angles of each link. (a) Trace of the movement of the end-effector. (b) Inverse joint angle of each link.

in (58). The tracking errors of each link are presented in Figs. 6(a), (b), and (c), where the error size of the proposed PFTSMC system is smaller than those of the other two systems. The estimated results for the first sliding mode surface of the FTSMC system given in (10) are presented in Figs. 6(d), (e), and (f). It is expected that the extended state observer of (22) can accurately estimate the unknown uncertainty from these results. For the designedσ_i, the prescribed control effectively constrains the rising effect of σ_i and the tracking error e_i, its rate $\dot{e}_i$ and the sliding surface s_i decrease indirectly. Thus, the tracking errors of the PFTSMC system can be made significantly smaller than those of the FTSMC by constraining the second sliding mode surface σ_i.

Finally, the control inputs of the PFTSMC system are presented in Fig. 6(j), where the second joint requires a higher control torque than the other joints because it should support the load of the third link including the load of the second link. Therefore, we showed through the experimental verfication that the proposed GWO-WOA technique offers a more advanced optimization performance than the conventional GWO and WOA techniques and that PFTSMC and the extended observer deliver outstanding performances.

7. CONCLUSION

In this study, a fractional-order nonsingular terminal sliding controller with prescribed control (PFTSMC), optimized by a hybrid GWO-WOA technique, was designed to achieve a more precise position tracking performance and faster controller design procedure for robotic manipulators. The improved PFTSMC offers a simpler prescribed control and extended state observer, and it also offers an improved GWO-WOA technique and experimental parameter optimization process, which could not be achieved in earlier bio-inspired optimization studies. This study enables a more precise motion control performance and an easier controller design for manipulator systems,

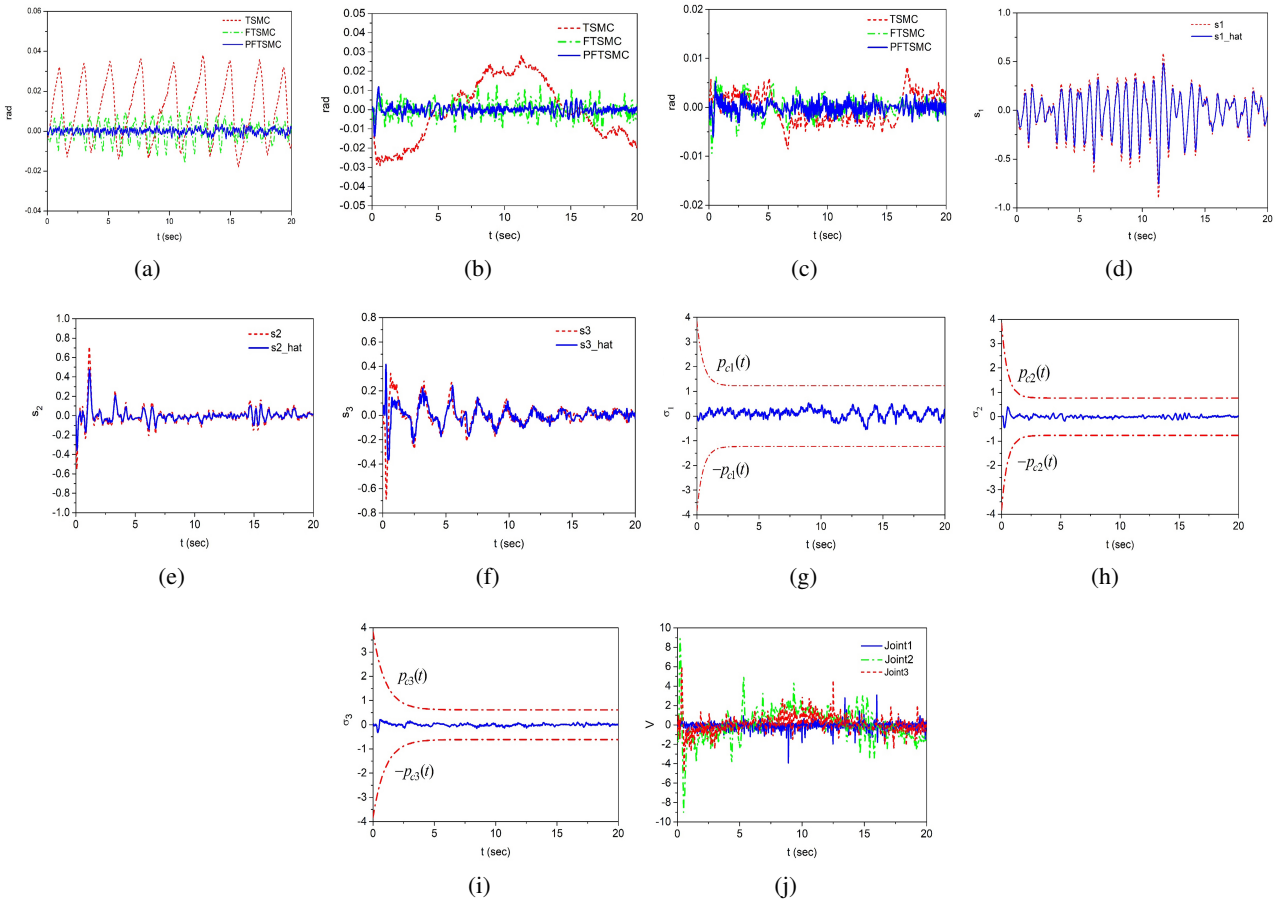

Fig. 6. Experimental results of the manipulator. (a) Joint angle tracking errors of link1. (b) Joint angle tracking errors of link2. (c) Joint angle tracking errors of link3. (d) Estimate $\hat{s}_1$. (e) Estimate $\hat{s}_2$. (f) Estimate $\hat{s}_3$. (g), (h), and (i) Prescribed function and for each link. (j) Control inputs of the PFTSMC system.

without consuming considerable amount of time and effort to tune the parameters of the control system through direct experimental optimization. As a next study, an automatic setting method for the parameter boundary limitation of the metaheuristic method combined with neural networks or fuzzy logic system is necessary.

REFERENCES

[1] X. Yan, K. Spurgeon, and C. Adward, "State and parameter estimation for nonlinear delay systems using sliding mode techniques," *IEEE Trans. Automatic Contr.*, vol. 58, no. 4, pp. 1023-2019, 2013.

[2] S. Yu, X. Yu, B. Shrinzadeh, and Z. Man, "Continuous finite-time control for robotic manipulators with terminal sliding mode," *Automatica*, vol. 41, pp. 1957-1964, 2005.

[3] H. Hou, X. Li, L. Xu, K. A. Rsetam, Z. Cao, "Finite-time continuous terminal sliding mode control of servo motor systems," *IEEE Trans. Industrial Electr.*, vol. 67, no. 7, pp. 5647-5656, 2020.

[4] L. Yang and J. Yang, "Nonsingular fast terminal sliding-mode control for nonlinear dynamical systems," *International J. of Robust and Nonlinear Contr.*, vol. 21, pp. 1865-1879, 2011.

[5] H. Wang, L. Shi, Z. Man, J. Zheng, and S. Li, "Continuous fast nonsingular terminal sliding mode control of automotive electronic throttle systems using finite-time exact observer," *IEEE Trans. Industrial Electr.*, vol. 65, no. 9, pp. 7160-7172, Sept. 2018.

[6] M. P. Aghababa, "Design of a chatter-free terminal sliding mode controller for nonlinear fractional-order dynamical system," *Inter. J. of Control*, vol. 86, no. 10, pp.1744-1756, 2013.

[7] H. R. Li, Z. B. Jiang, and N. Kang, "Sliding mode disturbance observer-based fractional second-order nonsingular terminal sliding mode control for PMSM position regulating system," *Mathematical Problems in Eng.*, vol. 2015, Arrticle ID 370904, 2015.

[8] Y. Wang, L. Gu, Y. Xu, and X. Cao, "Practical tracking control of robot manipulator with continuous fractional-order nonsingular terminal sliding mode," *IEEE Trans. Industrial Electr.*, vol. 63, no. 10, pp. 6194-6204, Oct. 2016.

[9] N. Ullah, M. A. Ali, A. Ideas, and J. Herrera, "Adaptive fractional order terminal sliding mode control of a doubly fed induction generator based wind energy system," *IEEE Access*, vol. 27, pp. 21368-21381, 2017.

[10] E. S. A. Shahri, A. Alfi, and J. A. T. Machado, "Stabilization of fractional-order systems subject to saturation element using fractional dynamic output feedback sliding mode control," *J. Computational and Nonlinear Dyn.*, vol. 12, no. 3, pp. 1274-1230, 2017.

[11] W. Yaoyao, J. Surong, C. Bai, and W. Hongtao, "A new continuous fractional-order nonsingular terminal sliding mode control for cable-driven manipulator," *Advances in Engineering Software*, vol. 119, pp. 21-29, 2018.

[12] S. Haghighatnia, H. T. Shandiz, and A. Alfi, "Conformable fractional order sliding mode control for a class of fractional order chaotic systems," *International J. Industrial Electronics Control and Opt.*, vol. 2, no. 3, pp. 177-188, 2019.

[13] J. A. Moreno and M. Osorio, "A Lyapunov approach to second-order sliding mode controller and observers," *Proc. of 47 th IEEE Confer. Decision and Contr.*, pp. 2856-2861, 2008.

[14] R. Poli, J. Kenndy, and T. Blackwell, "Particle swarm optimization," *Swarm Intelligence*, vol. 1, pp. 33-57, 2007.

[15] M. Dorigo and C. Blum, "Ant colony optimization theory: A survey," *Theoretical Computer Science*, vol. 344, pp. 243-278, 2005.

[16] D. Karaboga and B. Akay, "A comparative study of artificial bee colony algorithm," *Applied Mathematics and Comp.*, vol. 214, no. 1, pp. 108-132, 2009.

[17] O. Castillo and L. Amador-Angulo, "A generalized type-2 fuzzy logic approach for dynamic parameter adaptation in bee colony optimization applied to fuzzy controller design," *Information Science*, vol. 460, pp. 476-496, 2018.

[18] S. Mirjalili, S. M. Mirjalili, and A, Lewis, "Grey wolf optimizer," *Advances in Engineering Software,* vol. 69, pp. 46-61, 2014.

[19] L. Rodriguez, O. Castillo, M. Garcia, and J. Soria, "Constrained real-parameter optimization using the firefly algorithm and the grey wolf optimizer, hybrid Intelligent systems in control, pattern recognition, and medicine," *Studies in Computational Intelligence*, vol. 827, pp. 155-167, Springer, 2019.

[20] D. F. Sanchez, P. Melin, and O. Castillo, "A grey wolf optimizer for modular granular neural networks for human recognition,*? Computational Intelligence and Neuroscience*, vol. 2017, Article ID 4180510, 2017.

[21] J. Oliveira, P. M. Oliveira, J. Boaventura-Cunha, and T. Pinho, "Chaos-based grey wolf optimizer for higher order sliding mode position control of a robotic manipulator," *Nonlinear Dynamics*, vol. 90, no. 2, pp. 1353-1362, 2017.

[22] O. O. Obadina, M. Thaha, K. Althoefer, and M. H. Shaheed, "A modified computed torque control approach for a master-slave robot manipulator system," *Annual Confer. Towards Automation Robotic Sys.,* pp. 28-39, 2018.

[23] Z. Zhou, C. Wang, Z. Zhu, Y. Wang, and D. Yang, "Sliding mode control based on a hybrid grey-wolf-optimized extreme learning machine for robot manipulators," *Inter. J. for Light and Electron Optics*, vol. 185, pp. 364-380, 2019.

[24] H. Komijani, M. Masoumnezhad, M. M. Zanjireh, and M. Mir, "Robust hybrid fractional order proportional derivative sliding mode controller for robot manipulator based on extended grey wolf optimizer," *Robotica*, vol. 38, no. 4, pp. 605-616, 2020.

[25] S. Mirjalili, and A. Lewis, "The whale optimization algorithm," *Advances in Engineering Software*, vol. 95, pp. 51-67, 2016.

[26] J. H. Holland, "Genetic algorithm," *Scientific American*, vol. 267, no. 1, pp. 66-73, 1992.

[27] E. Rashedi, H. Nezamabadi, and S. Saryazdi, "GSA: A gravitational search algorithm," *Information Science,* vol. 179, no. 13, pp. 2232-2249, 2009.

[28] C. P. Benchlioulis and G. A. Rovithakis, "Robust adaptive control of feedback linearizable MIMO nonlinear systems with prescribed performance," *IEEE Trans. on Automatic Control,* vol. 53, no. 9, pp. 2090-2098, Oct. 2008.

[29] C. Hu, B. Yao, and Q. Wang, "Performance-oriented adaptive robust control of a class of nonlinear systems preceded by unknown deadzone with comparative experimental results," *IEEE/ASME Trans. Mechatronics,* vol. 18, no. 1, Feb. 2013.

[30] B. Bandyopadhyay and S. Kamal, *Stabilization and Control of Fractional Order Systems: A Sliding Mode Approach*, vol. 317, Springer, 2015.

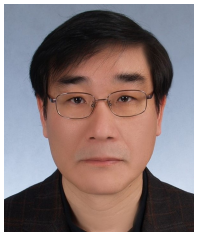

Seong-Ik Han received his B.S. and M.S. degrees in mechanical engineering from Pusan National University, Busan, Korea, in 1987 and 1989, respectively, and a Ph. D. in mechanical design engineering from Pusan National University, Busan, in 1995. From 1995 to 2009, he was with Electrical Automation of Suncheon First College, Korea. From 2010 to 2017, he was with the Department of Electronic Engineering, Pusan National University, Korea. Now, he is with the Department of Mechanical System Engineering, Dongguk University Gyeongju Campus, Korea. His research interests include intelligent control, nonlinear control, robotic control, vehicle system control, and steel process control. He is the member of IEEE. He has published 70 papers in the international journals as the first or corresponding author.